Electrochimica Acta 208 (2016) 25–32

Contents lists available at ScienceDirect

Electrochimica Acta

journal homepage: www.elsevier.com/locate/electacta

Perovskite-based bifunctional electrocatalysts for oxygen evolution and oxygen reduction in alkaline electrolytes

Karina Elumeeva[a,1], Justus Masa[a,1], Jennyfer Sierau[b], Frank Tietz[b], Martin Muhler[c], Wolfgang Schuhmann[a,1,*]

[a] Analytical Chemistry—Center for Electrochemical Sciences (CES), Ruhr-Universität Bochum, Universitätsstr. 150, D-44780 Bochum, Germany
[b] Forschungszentrum Jülich GmbH, IEK-1, D-52425 Jülich, Germany
[c] Laboratory of Industrial Chemistry, Ruhr-Universität Bochum, Universitätsstr. 150, D-44780 Bochum, Germany

ARTICLE INFO

Article history:
Received 1 October 2015
Received in revised form 1 May 2016
Accepted 2 May 2016
Available online 3 May 2016

Keywords:
Oxygen evolution reaction
Oxygen reduction reaction
Bifunctional electrocatalyst
Perovskite
Carbon nanotubes
Nitrogen-doped carbon nanotubes

ABSTRACT

Due to the high cost of precious metal-based electrocatalysts for oxygen reduction and oxygen evolution, the development of alternative low cost and efficient catalysts is of high importance for energy storage and conversion technologies. Although non-precious catalysts that can efficiently catalyze oxygen reduction and oxygen evolution have been developed, electrocatalysts with high bifunctional activity for both oxygen evolution and reduction are needed. Perovskites based on modified lanthanum cobaltite possess significant activity for the oxygen evolution reaction. We describe the synthesis of a bifunctional oxygen electrode with simultaneous activity for the oxygen evolution reaction (OER) and the oxygen reduction reaction (ORR) in alkaline media by direct growth of nitrogen-doped carbon nanotubes on the surface of a perovskite containing Co and Fe by means of chemical vapor deposition. The difference in the overvoltage between ORR (at 1 mA/cm^2) and OER (at 10 mA/cm^2) was below 880 mV in 0.1 M KOH. The formation of H_2O_2 during the ORR was reduced by at least three fold when using the bifunctional catalyst as compared to the non-modified perovskite. Long-term durability tests indicate stable performance for at least 37 h during the OER and 23 h during the ORR.

1. Introduction

Unitized regenerative fuel cells and metal-air batteries are among the most promising technologies for renewable energy conversion and storage. However, their large scale deployment is largely restricted by the unavailability of high performance and cost-effective bifunctional oxygen electrodes which can reversibly catalyze both the oxygen evolution reaction (OER) and the oxygen reduction reaction (ORR).

The routinely studied electrocatalysts for the ORR as well as the OER contain precious metals such as Pt, Pd, Ir and Ru [1–3] in acidic electrolytes. However, in addition to the scarcity of the materials which prevents their large scale application, the related catalysts suffer from low stability and sensitivity to poisoning. The development of non-noble metal or non-metal catalysts for the ORR [4–7] and the OER [3,8] was proposed. In particular, the ORR can be successfully catalyzed using a number of different materials including supported or non-supported oxides or metal nanoparticles [6,9,10], as well as nitrogen or heteroatom doped carbon that can be additionally modified by introducing transition metal cations [11,12]. The latter are the most active catalysts for substitution of precious-metal catalysts for ORR due to the presence of metal cations like Fe and Co coordinated to the nitrogen atoms incorporated in the carbon matrix. These N-coordinated metal ions are considered to serve as the main active sites, where oxygen can be adsorbed and reduced [6,11,13]. Furthermore, non-metal heteroatom-doped carbon materials (N, P, S, B) [7,14–16] also possess reasonable catalytic activity towards the ORR due to the charge delocalization in the carbon matrix yielding positively charged active species able to adsorb oxygen [15,17].

Among the electrocatalysts for OER, numerous transition metal compounds, e.g. oxides with perovskite structure (ABO_3), have received wide attention due to their high activity and durability for the OER especially when used in alkaline media [18–21]. Varying the type of rare or alkaline earth metal cations (A site) and *3d* transition metal cations (B sites) along with their ratio, their OER

* Corresponding author.
E-mail address: wolfgang.schuhmann@rub.de (W. Schuhmann).
[1] ISE member.

http://dx.doi.org/10.1016/j.electacta.2016.05.010
0013-4686/

activity can be substantially improved to become comparable to that of precious metals based benchmark catalysts [19,20,22,23]. Partial metal substitution can significantly influence not only the state of charge and distribution of ion vacancies within the perovskite structure but also its conductivity, and ultimately the OER performance [18,19,24,25].

Oxides with spinel and perovskite structures have been reported to exhibit bifunctional activity for both reactions. The transition metal cations can serve as a bifunctional active site for both ORR and OER depending on the potentials applied [10,21,26]. However, their activity for ORR is generally limited due to their low intrinsic conductivity. Hence, the main challenge on the way towards bifunctional oxygen electrodes is to combine catalytically active sites for OER and ORR into one highly effective bifunctional system. It was previously shown that one effective way to create bifunctional electrocatalysts is the integration of ORR and OER active materials into a composite which retains the individual properties [9,27] or forms new bifunctional active sites [2,28,29]. Catalysts in which ORR active sites are introduced into OER active materials or vice versa, may have advantages due to a better control of active site distribution. However, most of these composite materials exhibit a much higher activity for one reaction over the other, or they possess limited stability. Moreover, in addition of the minimization of the overpotential difference between the onset of OER and ORR it is at least similarly important to improve the longterm stability of the catalyst film, to favorably tune gas and electrolyte permeability and to assure a low resistance of the material [26].

We propose a comparatively simple approach for the modification of nanoparticles of a perovskite ($La_{0.58}Sr_{0.4}Fe_{0.2}Co_{0.8}O_3$) by growth of nitrogen-doped carbon nanotubes (NCNTs) on their surface using chemical vapor deposition (CVD) at comparatively low temperatures (below 700 °C). Due to the presence of metal ions (Fe, Co) the perovskite nanoparticles themselves can serve as catalyst for the NCNTs growth on their surface taking into account that mixed oxides of Fe/Co are the most used catalysts for the CVD growth of carbon nanotubes [30,31]. The growth of NCNTs on the perovskite surface significantly improved the activity of the composite catalysts with respect to the ORR. In contrast to previous reports, in which carbon deposits were grown on the modified surface of lanthanum nickelate [32] or lanthanum cobaltite [33,34] in the proposed procedure no pretreatment steps such as impregnation of the oxide with Fe or Co salts are necessary. The OER activity was found to be unchanged or slightly improved with respect to the unmodified perovskite, however, the ORR activity was substantially improved. The difference between overpotentials for OER and ORR measured at fixed current densities was considerably decreased and the materials exhibited high stability over the tested time period. It has to be emphasized that unlike the case for acidic media, carbon corrosion is much less investigated in alkaline electrolytes especially at conditions of the OER. Taking into consideration that the high applied potentials for the OER are beyond the stability of most known substances including noble metal oxides, it becomes evident that introducing enhanced conductivity into intrinsically non-conducting electrocatalysts is only possible using carbon based materials. Evidently, this might lead to a compromise of the stability of the new catalyst.

2. Experimental

2.1. Preparation of electrocatalysts

The perovskite $La_{0.58}Sr_{0.4}Fe_{0.2}Co_{0.8}O_3$ which was used as substrate and catalyst for NCNT growth was prepared via a citrate complexation technique. The nitrates of the respective metals (La, Sr, Co, Fe) in the required stoichiometric concentration were dissolved first in distilled water, then citric acid (CA) in the molar concentration of 2:1 (CA: metal salts) was added to the nitrate salts solution under intensive stirring for around 3 h at 80 °C. After this, ethylene glycol (EG) was added dropwise to the mixture (1 ml of EG to each 1 g of CA). The viscous mixture obtained was first dried at 230 °C for several hours, then calcined in air first at 600 °C for 3 h and then at 900 °C for 24 h. Samples were further milled in ethanol with zirconia balls.

Nitrogen-doped carbon deposits, mostly nanotubes, were grown on the perovskite nanoparticle surface using CVD. 100 mg of the perovskite powder was placed in a quartz boat that was inserted into the center of a tubular quartz reactor placed inside a 3-zone tube furnace with automatic temperature and gas flow control. First, pure N_2 was flushed into the reactor for 15 min, then the temperature was ramped at 10 °C min^{-1} until the synthesis temperature (640–680 °C) was reached under continuous N_2 flow (100 ml min^{-1}). After this, a C_2H_4/NH_3/He mixture (30:7:63 volume ratio, 100 ml min^{-1}) was passed through the reactor for 30 min. After the synthesis, the furnace was cooled down to room temperature under nitrogen atmosphere. The composite materials were used for physical and electrochemical characterization without any further treatment.

2.2. Physical characterization

Scanning electron microscopy (SEM) images were recorded using a Quanta 3D FEG scanning electron microscope (FEI™) operated at 20.0 kV. X-ray diffraction (XRD) studies were performed on a D4 Endeavour instrument (Bruker) using Cu-Kα radiation. Elemental analysis was performed using VarioEL III analyzer (Elementar Analysensysteme) to determine the concentration of C, N and H. Transmission electron microscopy (TEM) as well as energy-dispersive X-ray spectroscopy studies were carried out using a TECNAI G220 S-TWIN transmission electron microscope with LaB6-Cathode, 200 kV accelerating voltage and 0.24 nm point-resolution.

2.3. Electrochemical measurements

Electrochemical measurements were performed in a coaxial three-electrode cell. Glassy carbon rotating disk (RDE) and rotating ring-disk (RRDE) electrodes (4 mm and 5.6 mm diameter, respectively) modified with the catalyst film were used as working electrodes, a Ag/AgCl/3 M KCl was used as reference electrode and a platinum mesh as counter electrode. Catalyst inks were prepared using 5 mg of the catalyst powder dispersed in a mixture of ultrapure water, ethanol and Nafion solution (5 wt.%, Sigma Aldrich) with a volume ratio of 49:49:2. Inks were sonicated for at least 20 min to assure a homogeneous dispersion. RDEs were polished before each measurement with 1 μm and 0.3 μm alumina pastes. 5.3 μL and 10.6 μL of catalyst ink were cast onto the RDE and RRDE, respectively, and air dried to obtain a catalyst layer with a nominal loading of 210 μg cm^{-2}.

Electrochemical measurements were performed with an AutolabIII/FRA2 potentiostat (Metrohm-Autolab) with a RDE 710 rotator (Gamry Instruments) in oxygen saturated 0.1 M KOH as electrolyte. The coaxial cell geometry in which the working electrode is surrounded by the Pt mesh counter electrode and the RE is placed outside the counter electrode creates a symmetrical distribution of current lines. This diminishes the influence of the electrode position on the determination of the uncompensated solution resistance leading to a more precise determination of the ohmic drop [35]. Electrochemical impedance spectroscopy (EIS) was performed before each experiment at open circuit potential (OCP) using perturbation frequencies between 10 kHz and 200 Hz with an AC amplitude of 10 mV_{pp}. The electrolyte resistance was

derived from the real impedance axis of the Nyquist plots at high frequency, and was used for iR correction of the electrochemical data. Following this, a conditioning step was applied by continuous potential cycling between 0.1 and −0.5 V vs. Ag/AgCl/3 M KCl at a scan rate of 100 mV s^{-1} until reproducible voltammograms were obtained. This was typically achieved after 15-20 cyclic voltammograms. Finally, a linear sweep voltammogram in the potential range from 0.1 to −1 V and 0.1 V to +1 V vs. Ag/AgCl/3 M KCl with a scan rate of 5 mV s^{-1} were performed in order to evaluate the electrocatalytic properties of the catalysts for the ORR and OER, respectively. A rotation speed of 1600 rpm was used to avoid accumulation of evolved oxygen bubbles on the surface of the electrode. The ORR test was performed prior to the OER test to avoid the influence of bubble formation during the OER on the accuracy of the ORR measurements. All potentials were converted to the reversible hydrogen electrode scale (RHE). A bifunctionality parameter $\Delta E_{OER\text{-}ORR}$ was determined by subtracting the potential (iR corrected) corresponding to a current density of 10 mA cm^{-2} for OER from that corresponding to a current density of −1 mA cm^{-2} for ORR extracted from the linear sweep voltammogram. In RRDE experiments, the ring potential was set to 0.4 V vs. Ag/AgCl/3 M KCl. The yield of H_2O_2 and the number of transferred electrons (n) were calculated from the RRDE data according to the following equations:

$$H_2O_2(\%) = 200 \times \frac{I_R/N}{I_R/N + I_D}$$

$$n = 4 \times \frac{I_D}{I_R/N + I_D}$$

I_D and I_R are the disk and ring currents, respectively, and N is the collection efficiency determined for each modified catalyst film in 5 mM potassium ferrocyanide solution at 1600 rpm [36]. In the case of the RRDE measurements, a linear sweep voltammogram recorded in Ar-saturated electrolyte was subtracted from those recorded in oxygen saturated solution in order to correct for the influence of capacitive currents.

The *long-term durability* of the catalysts was assessed by galvanostatic and potentiostatic measurements in a specifically designed flow-through three-electrode electrochemical cell. Oxygen saturated 0.1 KOH solution was continuously pumped through the cell (50 mL min^{-1}). A graphite rod of 5 mm in diameter modified with the catalyst ink was used as working electrode. Catalyst inks for the stability measurements were prepared in the same way as for RDE and RRDE experiments; however, the catalyst loading was increased to 530 μg cm^{-2} in order to obtain homogeneous catalytic films on the surface of a graphite electrode.

Galvanostatic polarization measurements were performed at a fixed current of 2 mA (around 10.2 mA cm^{-2}) to determine the catalyst stability during OER. The stability test involved a repeating sequence of galvanostatic polarization for 0.5 h followed by stabilization and EIS measurements. The EIS data were used for iR correction of the acquired chronopotentiometric data.

Potentiostatic measurements were performed at −0.4 V (vs. Ag/AgCl/3 M KCl) to investigate the ORR stability of the catalytic systems. The stability measurement was performed for 23 h with interruptions for stabilization and EIS measurements. A conditioning step was performed prior to the stability measurements by sweeping the potential between 0.1 to −0.6 V vs. Ag/AgCl/3 M KCl at 100 mV s^{-1} until reproducible voltammograms were obtained (typically at least 15-20 cycles).

3. Results and discussion

3.1. Influence of the synthesis temperature on the morphology and composition of NCNT-modified perovskite electrocatalysts

SEM, HRTEM and XRD were used to investigate the effect of the temperature of the CVD process on the morphological and

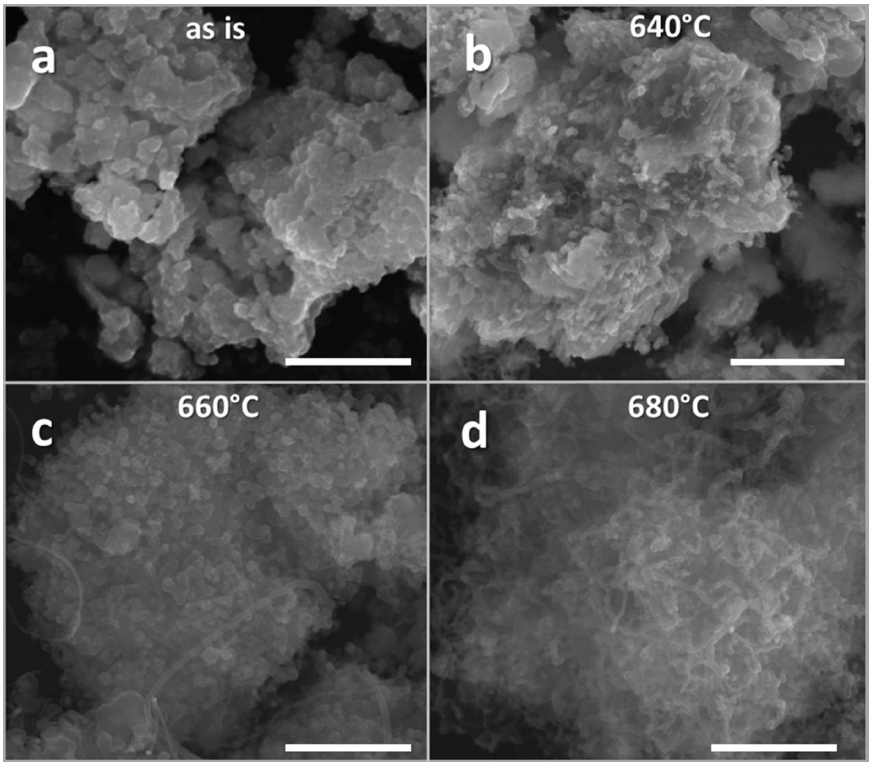

Fig. 1. SEM images of the pure perovskite before NCNTs growth (a), and after CVD growth of NCNTs at 640 °C (b), 660 °C (c), 680 °C (d) (scale bar is 1 μm).

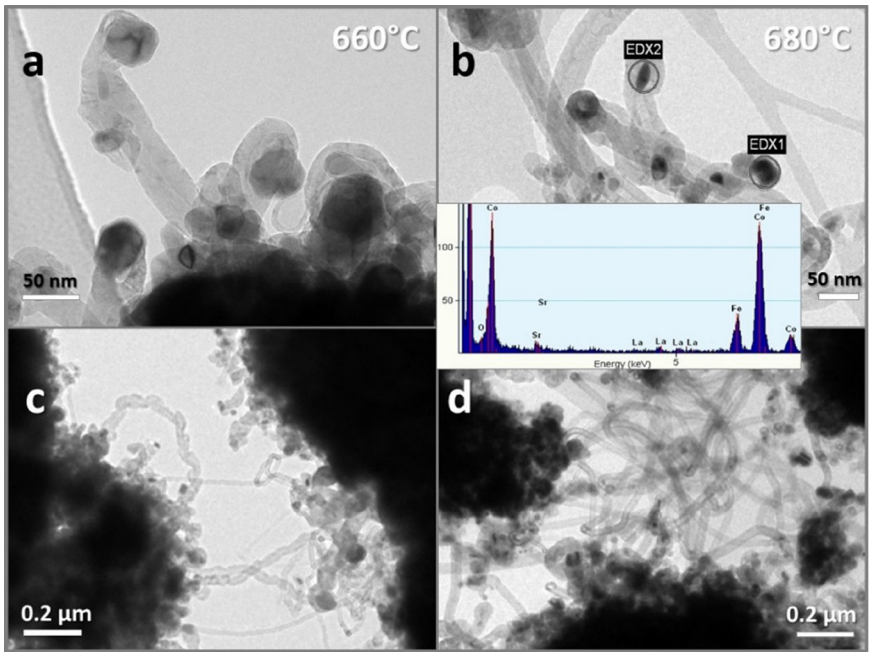

Fig. 2. High (a,b) and low (c,d) resolution TEM images of perovskite/NCNTs composite materials prepared by the CVD at 660 °C (a,c) and 680 °C (b,d). Inset in (b) shows the EDX analysis of the metal particles encapsulated in the NCNTs core.

structural properties of NCNT-modified perovskites. All synthesis conditions, including gas composition, flow rate and duration were optimized (data not shown).

SEM images reveal that the starting material ($La_{0.58}Sr_{0.4}Fe_{0.2}Co_{0.8}O_3$) consists of rather large flat particles (Fig. 1a). After exposure of the perovskite to the carbon and nitrogen precursor ($C_2H_4/NH_3/He$) at temperatures higher than 600 °C, carbon deposits are formed on the perovskite particle surface (Fig. 1b–d). Treatment at 640 °C leads to the formation of short carbon nano-structures with a rather low density (Fig. 1b) with the initial morphology of the perovskite particles being unchanged. At 660 °C carbon is deposited more densely, however, mostly short structures with a length of 300–400 nm are formed (Fig. 1c). At 680 °C longer nanotubes with a dense coverage of the individual perovskite particles are obtained (Fig. 1d). Evidently, a small temperature change can significantly modulate the morphological properties of the formed carbon structures on the perovskite surface [30,31]. At temperatures higher than 600 °C, the metal cations are reduced under formation of small metal nanoparticles which are the reaction sites for the formation of carbon nanotubes (CNTs). A temperature increase during CVD deposition of CNTs leads to rapid reduction of the oxide and metal particle sintering resulting in the formation of CNTs with larger diameters. At the temperature employed, NCNTs with 30–50 nm diameter are formed. Their dimensions did not change significantly with changing the deposition temperature. Improved carbon diffusion or faster ethylene decomposition may explain the preferential formation of longer nanotubes at 680 °C.

The tubular structure of the carbon deposits obtained on the perovskite surface was confirmed by HRTEM (Fig. 2). At both 660 and 680 °C, the formed CNTs have rather thick walls indicating the presence of large number of single graphitic shells with the length being sufficiently larger at 680 °C. Moreover, at 680° C (Fig. 2b, d) the metal nanoparticles encapsulated within the graphitic shell are barely visible in the high resolution images. EDX analysis of the particles encapsulated inside the CNT core confirmed the presence of both Fe and Co. The perovskite surface gets reduced under the ethylene flow and releases part of Fe and Co cations forming a Fe-Co alloyed nanoparticles on the Sr- and La-enriched surfaces. The presence of N atoms in the perovskite-CNT composites was confirmed by elemental analysis (Table 1). The N concentration was found to be rather low (1–2 wt.%) for all samples with the C:N ratio being almost the same for the samples prepared at 660 and 680 °C.

Table 1
Elemental analysis* of the perovskite sample modified with NCNTs grown at different temperatures (640 to 680 °C).

Sample	N	C	H	C/N ratio
NCNT-640	2.3	16.8	0.7	7.3
NCNT-660	1.05	25.6	0.7	24.3
NCNT-680	1.4	35.0	0.8	25.0

*Weight %.

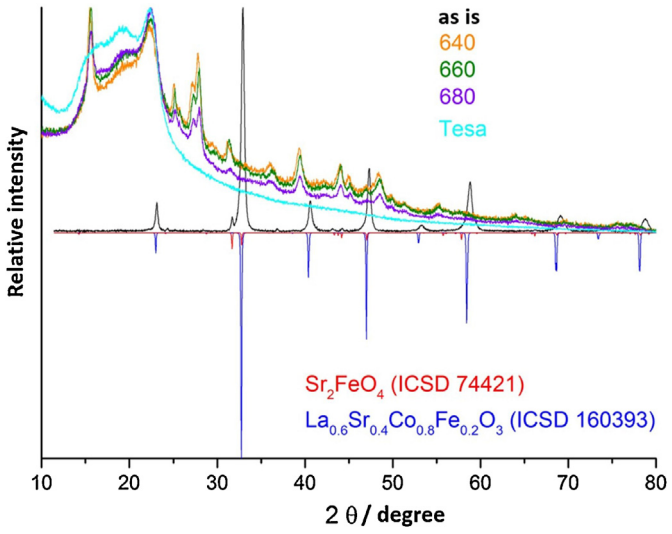

Fig. 3. XRD patterns of the pure perovskite (black line) and after NCNTs growth at different temperatures (orange – 640 °C, green – 660 °C, violet – 680 °C). Two model patterns from the ISCD database are presented for comparison (dark blue and red lines). Tesa is an adhesive tape used for fixation of the sample (cyan line).

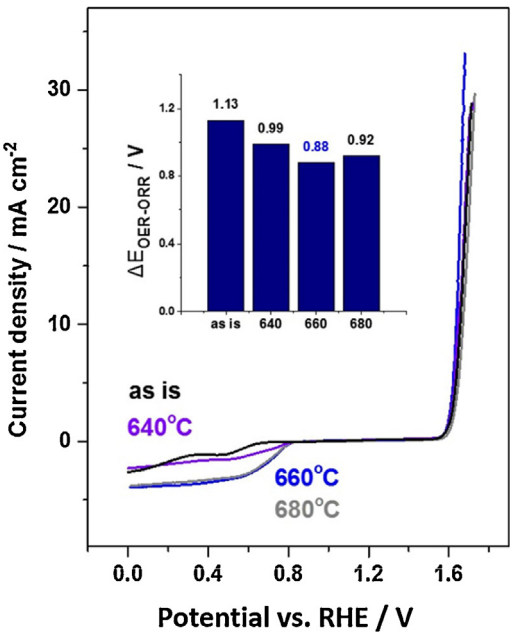

Fig. 4. Bifunctional electrocatalytic activity of perovskite-based catalysts before and after CVD growth of NCNTs, measured in O_2 saturated 0.1 M KOH at a scan rate of 5 mV s^{-1} and 1600 rpm electrode rotation (iR compensated). Inset: bifunctionality parameter determined as the difference between OER and ORR overpotentials at +10 mA cm^{-2} and −1 mA cm^{-2}, respectively.

In the XRD pattern of the non-treated perovskite sample, diffraction peaks corresponding to $La_{0.6}Sr_{0.4}Fe_{0.2}Co_{0.8}O_3$ predominate (Fig. 3). A low intensity peak at around 31.1° is visible and corresponds to the Sr_2FeO_4 phase. After the NCNT growth the crystalline structure of the perovskite is completely changed and peak assignment of the corresponding XRD pattern is complicated. The clear reflection at around 26° is attributed to the formation of CNTs. The other reflections could be from mixed oxides of the general composition $(La_xSr_y)_2(Co_vFe_w)O_4$ with x, y, v and w between 0 to 1. In general, we cannot exclude the influence of phase compositional changes on the formation and distribution of catalytically active sites of the developed systems.

3.2. Electrochemical evaluation of bifunctional catalytic activities for ORR and OER

Figs. 4 and 5 show the bifunctional electrocatalytic activity as well as O_2 reduction selectivity of the perovskite/NCNT-based catalysts. RDE and RRDE measurements were performed in O_2 saturated 0.1 M KOH under rotation at 1600 rpm. The pristine perovskite exhibits good catalytic performance towards OER. Lanthanum cobaltites generally possess high OER activity which can be tuned and improved by partial atom substitution [18,23–25]. However, the ORR activity is rather low as shown in Fig. 4. In contrast, electrodes modified with composite materials of the same perovskite with NCNTs exhibit a substantially improved catalytic activity for ORR. This may be due to an enhanced charge transport owing to the high conductivity of the NCNTs as well as the inherent high activity of NCNTs for ORR [37]. Hence, different types of active sites for ORR can be supposed, namely metal cations coordinated to the N atoms incorporated into the carbon matrix, metal oxide or metal nanoparticles formed during the CVD treatment, and carbon atoms adjacent to the nitrogen atoms in the carbon structure [15,17]. In the case of the OER activity careful control of the synthesis conditions allowed us to retain and even slightly improve the OER performance of the perovskite/NCNTs-based electrocatalysts (Fig. 4). Samples treated at 640 and 660 °C showed a slight shift of the OER overpotential at a given current density to more negative values which may at least partially be attributed to an improved conductivity. However, the actual nature and structure of the oxygen evolving active sites after the CVD modification remains to be clarified. We anticipate that N-doped carbon coordinated to Co may be most likely the active sites for the observed enhanced ORR activity. Together with the enhanced electronic conductivity and the observed modulations of the phase composition also the slightly enhanced OER activity may be explained. Importantly, the perovskite particles surface is not completely covered with NCNTs in the case of samples prepared at 640 or 660 °C. Hence, reactants may be able to access active sites of

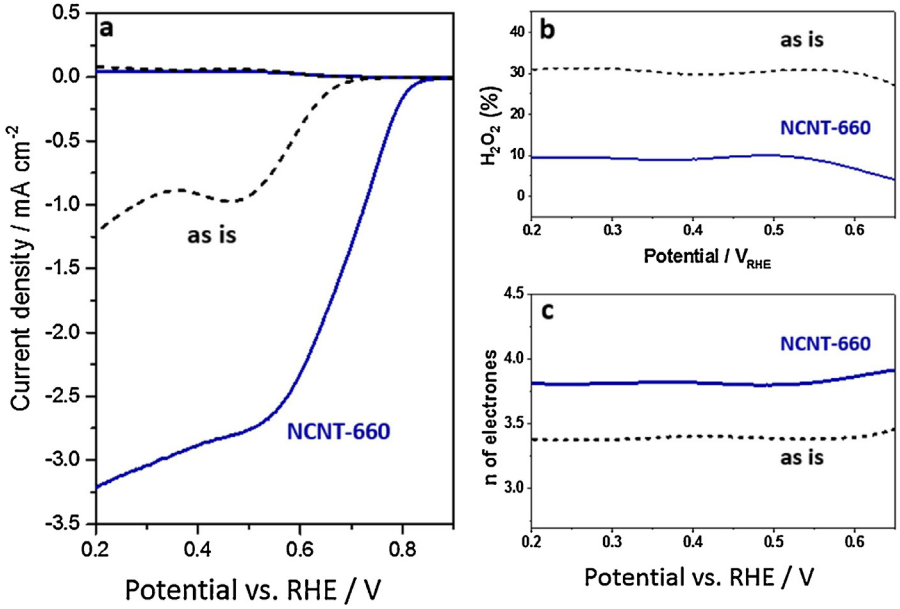

Fig. 5. Rotating ring-disk electrode measurements of the pure perovskite and the perovskite/NCNTs composite material prepared at 660 °C. The disk polarization curves were recorded at a scan rate of 5 mV s^{-1} and 1600 rpm electrode rotation, while the ring was held at a constant potential of 1.37 V (vs RHE) (a), H_2O_2 yield in % (b), number of transferred electrons (c). The collection efficiency for calibrated for all individual electrodes and was between 30-31%.

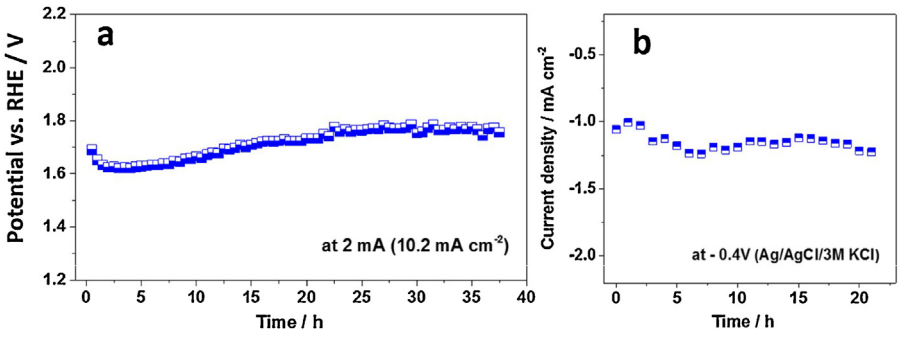

Fig. 6. Long-term stability tests of the perovskite/NCNTs composite material prepared at 660 °C using a graphite electrode (d = 5 mm). a) Galvanostatic polarization at 10.2 mA cm^{-2} depicting the OER stability, b) chronoamperometry at a constant potential of 0.57 V (vs RHE) in a flow-through cell with continuous circulation of O_2 saturated 0.1 M KOH depicting the ORR stability.

the perovskite surface even after their modification by CVD treatment. In the case of the sample which was obtained at a temperature of 680 °C, NCNTs cover the perovskite particles more densely. This may explain the observed higher overpotential for the OER for which access to the catalytic sites at the perovskite surface is indispensable (Fig. 4). The difference in the overpotentials for ORR and OER ($\Delta E_{OER-ORR}$) significantly changes with increasing NCNTs synthesis temperature with the composite material synthesized at 660 °C showing the lowest value.

Rotating ring-disk electrode (RRDE) measurements in the potential range of ORR showed low ring currents for the pure perovskite as well as for the perovskite/NCNTs composite synthesized at 660 °C (Fig. 5a). The maximum percentage of H_2O_2 produced during the ORR was 30% in the case of the pure perovskite (Fig. 5b) and below 10% for the perovskite/NCNTs composite (Fig. 5c) indicating improved selectivity favoring the 4 electron transfer pathway during ORR. A H_2O_2 yield of 10% is higher than reported for Pt-based catalysts, however, this value compares favorably with the H_2O_2 yield of typical non-precious catalysts in alkaline electrolytes [5].

3.3. Galvanostatic and potentiostatic stability tests

High stability of a bifunctional catalyst system during ORR and OER is one of the key parameters for possible future applications. The stability of the synthesized composite materials was evaluated by means of chronopotentiometry at a constant current density of 10 mA cm^{-2} for the OER and by means of chronoamperometry at a constant potential of 0.57 V (vs RHE) for ORR (Fig. 6). The stability measurements were performed in a custom-designed three-electrode flow-through electrochemical cell in a continuously pumped through 0.1 M KOH solution to remove gas bubbles from the catalyst modified electrode surface. A graphite electrode modified with the perovskite/NCNTs composite material synthesized at 660 °C was used as working electrode. Graphite electrodes are superior to glassy carbon electrodes in stability tests as detachment of the catalyst film caused by strong bubble formation is reduced. Results of the stability test for the OER are shown in Fig. 6a. During the initial ~5 h the electrode exhibited an increase in activity due to activation of the composite material. A slow degradation in the activity at the rate of 6–7 mV h^{-1} was observed between 5 and 20 h of continuous polarization reaching a potential plateau of ~1.7 V between 20 and 37 h. The small fluctuations in the recorded potential values result from bubble growth and departure and hence a continuous modulation of the accessible surface area. EIS measurements performed before each galvanostatic polarization time showed only slight deviations in the ohmic resistance (18–20 Ω).

Chronoamperometric stability measurements at 0.57 V (vs RHE) for ORR show no current decline during 23 h (Fig. 6b). During the first 2 h, the current density was slightly lower, however, after 3 h a plateau was reached, and the current did not significantly change for up to 23 h of the ORR stability test. To preclude the possibility of ORR activity enhancement due to Pt dissolution from the counter electrode and re-deposition at the working electrode, two control experiments were performed. In the first control experiment, the Pt counter electrode was located in a compartment separated with a glass frit from the WE and RE compartment. The stability data acquired in this measurement over 9 h of constant polarization at 0.57 V was compared with data acquired in the same set-up but without a frit separating the two compartments. We observed the same trend in both cases, and no

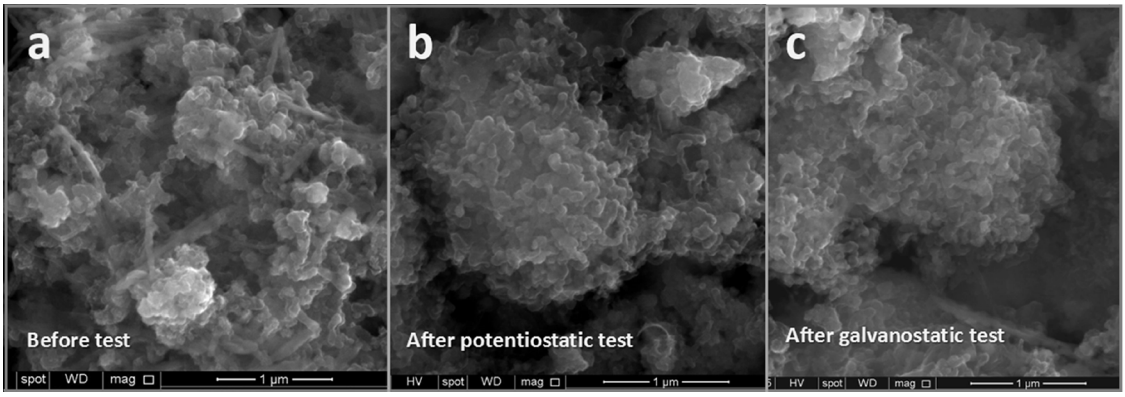

Fig. 7. SEM images of a bifunctional catalyst film mixed with Nafion as a binder: a) as deposited, b) after potentiostatic stability tests for 23 h at 0.57 V (vs. RHE), and c) after galvanostatic stability tests for 37 h at a current density of 10 mA cm^{-2} performed in a flow-through cell with O_2-saturated 0.1 M KOH as electrolyte.

systematic activation or current increase was observed in the set-up with the non-compartmentalized cell. Pt dissolution at the counter electrode obviously does not occur at the applied potential (0.57 V_{RHE}), and hence the possibility of Pt promoting the ORR activity can be excluded. Nonetheless, employing modern techniques for probing Pt dissolution, for example, the use of an electrochemical flow-cell coupled to ICP-MS for real-time online monitoring of dissolved Pt might perhaps reveal deeper insight of the possibility of Pt dissolution at the counter electrode, and its deposition at the working electrode during chronoamperometric ORR stability measurements [38]. In a second control experiment the potential of the Pt counter electrode was monitored during potentiostatic polarization of the catalyst modified electrode to the ORR potential of 0.57 V_{RHE}. The counter electrode potential was constant exhibiting only marginal variations at around 0.76 V vs SHE. At this potential, Pt dissolution should not occur in the used alkaline electrolyte at a pH value of 13 based on the Pourbaix diagram for bulk Pt [39]. This further provides evidence that the increased ORR activity of the NCNT-modified perovskite is solely due to the introduction of new Co-N-C active sites excluding any Pt dissolution and re-precipitation from the counter electrode.

In order to possibly apply carbon containing catalysts in real devices, a thorough investigation of the corrosion and degradation behavior of carbon is imperative. However, unlike in acidic electrolytes [40,41] carbon corrosion in alkaline electrolytes especially during longterm OER test was not yet elucidated at the required level. Evidently, to investigate carbon corrosion in alkaline media is beyond the scope of this work, however, SEM images shown in Fig. 7 demonstrate that after 23 h of potentiostatic polarization (Fig. 7b) and 37 hours of galvanostatic polarization (Fig. 7c) the carbon nanotube structure on the perovskite surface did not substantially change as compared to the pristine material (Fig. 7a).

4. Conclusions

The synthesis of a perovskite/NCNT composite material at an optimized CVD temperature of 660 °C provided access to a bifunctional electrocatalyst able to catalyze both ORR and OER with high activity and promising durability. Active sites for the ORR were introduced into the perovskite which exhibits intrinsically high OER activity by direct CVD growth of NCNTs on the surface of the perovskite without any pre- and post-treatment steps. Careful control of the synthesis parameters allowed us to retain and even improve the OER performance of the obtained composite material while introducing substantially enhanced ORR activity. We successfully demonstrated a novel concept of using perovskite-type mixed oxide as catalysts for the direct growth of NCNTs firmly attached on the surface of the catalyst particles and simultaneously introducing a second catalytic function, in this case, catalytic sites for the ORR. The question of possible carbon corrosion in alkaline electrolytes remains of concern and needs to be explored in detail to assess the practical viability of such catalysts in real devices under long-term operation.

Acknowledgements

Financial support from the Cluster of Excellence RESOLV (EXC 1069) funded by the DFG (Deutsche Forschungsgemeinschaft) and in the framework of Helmholtz-Energie-Allianz “Stationäre elektrochemische Speicher und Wandler” (HA-E-0002) is gratefully acknowledged. The authors are grateful to S. Selve (TU Berlin) for TEM measurements.

References

[1] T. Reier, M. Oezaslan, P. Strasser, Electrocatalytic oxygen evolution reaction (OER) on Ru, Ir, and Pt catalysts, ACS Catalysis 2 (2012) 1765–1772.
[2] G. Zhang, Z.-G. Shao, W. Lu, G. Li, F. Liu, B. Yi, One-pot synthesis of Ir@Pt nanodendrites as highly active bifunctional electrocatalysts for oxygen reduction and oxygen evolution in acidic medium, Electrochemistry Communications 22 (2012) 145–148.
[3] E. Fabbri, A. Habereder, K. Waltar, R. Kötz, T.J. Schmidt, Developments and perspectives of oxide-based catalysts for the oxygen evolution reaction, Catalysis Science & Technology 4 (2014) 3800–3821.
[4] F. Jaouen, E. Proietti, M. Lefèvre, R. Chenitz, J.-P. Dodelet, G. Wu, H.T. Chung, C. M. Johnston, P. Zelenay, Recent advances in non-precious metal catalysis for oxygen-reduction reaction in polymer electrolyte fuel cells, Energy & Environmental Science 4 (2011) 114–130.
[5] Y. Nie, L. Li, Z. Wei, Recent advancements in Pt and Pt-free catalysts for oxygen reduction reaction, Chemical Society Reviews 44 (2015) 2168–2201.
[6] Z. Chen, D. Higgins, A. Yu, L. Zhang, J. Zhang, A review on non-precious metal electrocatalysts for PEM fuel cells, Energy & Environmental Science 4 (2011) 3167.
[7] D. Yu, E. Nagelli, F. Du, L. Dai, Metal-free carbon nanomaterials become more active than metal catalysts and last longer, Journal of Physical Chemistry Letters 1 (2010) 2165–2173.
[8] C.C.L. McCrory, S. Jung, J.C. Peters, T.F. Jaramillo, Benchmarking heterogeneous electrocatalysts for the oxygen evolution reaction, Journal of the American Chemical Society 135 (2013) 16977–16987.
[9] J. Masa, W. Xia, I. Sinev, A. Zhao, Z. Sun, S. Grützke, P. Weide, M. Muhler, W. Schuhmann, Mn(x)O(y)/NC and Co(x)O(y)/NC nanoparticles embedded in a nitrogen-doped carbon matrix for high-performance bifunctional oxygen electrodes, Angewandte Chemie (International ed.) 53 (2014) 8508–8512.
[10] Y. Gorlin, T.F. Jaramillo, A bifunctional nonprecious metal catalyst for oxygen reduction and water oxidation, Journal of the American Chemical Society 132 (2010) 13612–13614.
[11] M. Lefèvre, E. Proietti, F. Jaouen, J.P. Dodelet, Iron-based catalysts with improved oxygen reduction activity in polymer electrolyte fuel cells, Science 324 (2009) 71–74.
[12] J. Masa, A. Zhao, W. Xia, M. Muhler, W. Schuhmann, Metal-free catalysts for oxygen reduction in alkaline electrolytes, Electrochimica Acta 128 (2014) 271–278.
[13] K. Elumeeva, J. Ren, M. Antonietti, T.-P. Fellinger, High surface iron/cobalt-containing nitrogen-doped carbon aerogels as non-precious advanced electrocatalysts for oxygen reduction, ChemElectroChem 2 (2015) 584–591.
[14] S. Chen, J. Bi, Y. Zhao, L. Yang, C. Zhang, Y. Ma, Q. Wu, X. Wang, Z. Hu, Nitrogen-doped carbon nanocages as efficient metal-free electrocatalysts for oxygen reduction reaction, Advanced materials 24 (2012) 5593–5597.
[15] K. Elumeeva, N. Fechler, T.P. Fellinger, M. Antonietti, Metal-free ionic liquid-derived electrocatalyst for high-performance oxygen reduction in acidic and alkaline electrolytes, Materials Horizons 1 (2014) 588–594.
[16] C.H. Choi, S.H. Park, S.I. Woo, Binary and ternary doping of nitrogen, boron, and phosphorus into carbon for enhancing electrochemical oxygen reduction activity, ACS Nano 6 (2012) 7084–7091.
[17] K. Gong, F. Du, Z. Xia, M. Durstock, L. Dai, Nitrogen-doped carbon nanotube arrays with high electrocatalytic activity for oxygen reduction, Science 323 (2009) 760–764.
[18] R.A. Rincón, E. Ventosa, F. Tietz, J. Masa, S. Seisel, V. Kuznetsov, W. Schuhmann, Evaluation of perovskites as electrocatalysts for the oxygen evolution reaction, ChemPhysChem 15 (2014) 2810–2816.
[19] A. Grimaud, K.J. May, C.E. Carlton, Y.-L. Lee, M. Risch, W.T. Hong, J. Zhou, Y. Shao-Horn, Double perovskites as a family of highly active catalysts for oxygen evolution in alkaline solution, Nature Communications 4 (2013) 2439.
[20] J. Suntivich, K.J. May, H.A. Gasteiger, J.B. Goodenough, Y. Shao-Horn, A perovskite oxide optimized for oxygen evolution catalysis from molecular orbital principles, Science 334 (2011) 1383–1385.
[21] W.G. Hardin, D.A. Slanac, X. Wang, S. Dai, K.P. Johnston, K.J. Stevenson, Highly active, nonprecious metal perovskite electrocatalysts for bifunctional metal-air battery electrodes, Journal of Physical Chemistry Letters 4 (2013) 1254–1259.
[22] K.J. May, C.E. Carlton, K.A. Stoerzinger, M. Risch, J. Suntivich, Y.-L. Lee, A. Grimaud, Y. Shao-Horn, Influence of oxygen evolution during water oxidation on the surface of perovskite oxide catalysts, Journal of Physical Chemistry Letters 3 (2012) 3264–3270.
[23] K. Elumeeva, J. Masa, F. Tietz, F. Yang, W. Xia, M. Muhler, W. Schuhmann, A simple approach towards high-performance perovskite-based bifunctional oxygen electrocatalysts, ChemElectroChem 3 (2016) 138–143.
[24] Y. Matsumoto, S. Yamada, T. Nishida, E. Sato, Oxygen evolution on $La_{1-x}Sr_xFe_{1-y}Co_yO_3$ series oxides, Journal of the Electrochemical Society 127 (1980) 2360–2364.
[25] S.K. Tiwari, S.P. Singh, R.N. Singh, Effects of Ni, Fe, Cu, and Cr substitutions for Co in $La_{0.8}Sr_{0.2}CoO_3$ on electrocatalytic properties for oxygen evolution, Journal of the Electrochemical Society 143 (1996) 1505–1510.
[26] S.W. Price, S.J. Thompson, X. Li, S.F. Gorman, D. Pletcher, A.E. Russell, F.C. Walsh, R.G. Wills, The fabrication of a bifunctional oxygen electrode without carbon components for alkaline secondary batteries, Journal of Power Sources 259 (2014) 43–49.

[27] R.A. Rincón, J. Masa, S. Mehrpour, F. Tietz, W. Schuhmann, Activation of oxygen evolving perovskites for oxygen reduction by functionalization with Fe-N(x)/C groups, Chemical Communications 50 (2014) 14760–14762.
[28] J. Zhang, Z. Zhao, Z. Xia, L. Dai, A metal-free bifunctional electrocatalyst for oxygen reduction and oxygen evolution reactions, Nature Nanotechnology 10 (2015) 444–452.
[29] G.-L. Tian, M.-Q. Zhao, D. Yu, X.-Y. Kong, J.-Q. Huang, Q. Zhang, F. Wei, Nitrogen-doped graphene/carbon nanotube hybrids: in situ formation on bifunctional catalysts and their superior electrocatalytic activity for oxygen evolution/reduction reaction, Small 10 (2014) 2251–2259.
[30] J.-P. Tessonnier, D.S. Su, Recent progress on the growth mechanism of carbon nanotubes: a review, ChemSusChem 4 (2011) 824–847.
[31] V.L. Kuznetsov, D.V. Krasnikov, A.N. Schmakov, K.V. Elumeeva, In-situ and ex-situ time resolved study of multi-component Fe-Co oxide catalyst activation during MWNT synthesis, Physica Status Solidi B 249 (2012) 2390–2394.
[32] Z. Chen, A. Yu, D. Higgins, H. Li, H. Wang, Z. Chen, Highly active and durable core-corona structured bifunctional catalyst for rechargeable metal-air battery application, Nano Letters 12 (2012) 1946–1952.
[33] D. Thiele, E. Lopez-Camacho Colmenarejo, B. Grobety, A. Züttel, Synthesis of carbon nanotubes on $La_{0.6}Sr_{0.4}CoO_3$ as substrate, Diamond and Related Materials 18 (2009) 34–38.
[34] A. Weidenkaff, S.G. Ebbinghaus, T. Lippert, $Ln_{1-x}A_xCoO_3$ (Ln = Er, La; A = Ca Sr)/carbon nanotube composite materials applied for rechargeable Zn/Air batteries, Chemistry of Materials 14 (2002) 1797–1805.
[35] A. Battistel, M. Fan, J. Stojadinović, F. La Mantia, Analysis and mitigation of the artefacts in electrochemical impedance spectroscopy due to three-electrode geometry, Electrochimica Acta 135 (2014) 133–138.
[36] U.A. Paulus, T.J. Schmidt, H.A. Gasteiger, R.J. Behm, Oxygen reduction on a high-surface area Pt:vulcan carbon catalyst: a thin-film rotating ring-disk electrode study, Journal of Electroanalytical Chemistry 495 (2001) 134–145.
[37] J. Masa, W. Xia, M. Muhler, W. Schuhmann, On the role of metals in nitrogen-doped carbon electrocatalysts for oxygen reduction, Angewandte Chemie (International ed.) 54 (2015) 10102–10120.
[38] A.A. Topalov, S. Cherevko, A.R. Zeradjanin, J.C. Meier, I. Katsounaros, K.J.J. Mayrhofer, Towards a comprehensive understanding of platinum dissolution in acidic media, Chemical Science 5 (2014) 631.
[39] V. Tripkovic, I. Cerri, t. Nagami, T. Bligaard, J. Rossmeisl, Platinum redispersion on metal oxides in low temperature fuel cells, Physical Chemistry Chemical Physics 15 (2013) 3279.
[40] L.M. Roen, C.H. Paik, T.D. Jarvi, Electrocatalytic Corrosion of Carbon Support in PEMFC Cathodes, Electrochemical and Solid-State Letters 7 (2004) A19–A22.
[41] J.P. Meyers, R.M. Darling, Model of Carbon Corrosion in PEM Fuel Cells, Journal of the Electrochemical Society 153 (2006) A1432–A1439.